Optical properties of ZnO/(Zn, Mg)O quantum wells

Thierry BRETAGNON[1,2,*]

[1]Charles Coulomb Laboratory, UMR5221, Montpellier 2 University, Montpellier, France
[2]Charles Coulomb Laboratory, UMR5221, National Center for Scientific Research (CNRS),
Montpellier, France

Abstract: This paper reviews the optical properties of ZnO/(Zn, Mg)O single quantum wells grown by molecular beam epitaxy. Both heteroepitaxial quantum well growth along the polar c-direction and homoepitaxial quantum well growth on the nonpolar M plane cases are considered. The optical properties of these quantum wells are investigated by using reflectance, continuous wave photoluminescence, and time-resolved photoluminescence spectroscopies. The quantum-confined Stark effect dominates the properties of the excitons for polar quantum wells. The magnitude of the internal electric field that is induced by both spontaneous and piezoelectric polarizations is determined by comparing the experimental results with a variational calculation of excitonic energies and lifetimes. For nonpolar quantum wells, the optical spectra reveal strong in-plane optical anisotropies, as predicted by the group theory. Moreover, the radiative recombination of free excitons is dominating the quantum well photoluminescence even at room temperature.

Key words: ZnO, quantum wells, quantum-confined Stark effect, nonpolar quantum wells

1. Introduction

Zinc oxide (ZnO) is a II–VI semiconductor compound that has numerous potential applications [1]. ZnO crystallizes preferentially in the hexagonal structure [1,2] and its wide band gap of 3.27 eV is close to that of gallium nitride (GaN – 3.42 eV). ZnO and related compounds have gained a renewed interest for optoelectronic applications owing in part to the fact that ZnO/(Zn, Mg)O quantum wells (QWs) have been successfully grown by laser-assisted molecular-beam epitaxy (LMBE) [3][4]. GaN-based materials have demonstrated their potential in blue/green light emitting diodes and laser diodes. However, ZnO still receives particular attention because of its large exciton binding energy ($\sim$60 meV), which can offer the possibility of efficient excitonic mechanisms operating at room temperature.

Band gap engineering is one of the crucial issues for device applications. It could be achieved by using magnesium or cadmium to make (Zn, Mg)O or (Zn, Cd)O. For example, the band gap energy at room temperature increases from 3.27 eV for ZnO to $\sim$3.87 eV for 33% magnesium in the alloy [5], with a fairly small lattice mismatch between the binary and ternary compounds.

ZnO/(Zn,Mg)O QWs have been successfully grown by different techniques such as LMBE [6–10], metal–organic chemical vapor deposition [11,12], and molecular beam epitaxy (MBE) [13–15]. Originally sapphire [3] substrates were used. To grow ZnO and its related alloys, other substrates such as SCAM, Si(111), and GaN

---

*Correspondence: thierry.bretagnon@univ-montp2.fr

have been successfully used since then. Optical and structural properties were recently improved when the ZnO/(Zn, Mg)O heterostructures were grown by MBE using ZnO substrates [16].

Internal electric fields were found to appear naturally in strained group III-nitride-based quantum structures grown along the c-direction. Despite the fact that theoretical calculations [17,18] of the polarization properties in ZnO and (Zn, Mg)O predict larger spontaneous and piezoelectric constants than for GaN-based systems, the first experimental results reported [19] on ZnO/(Zn, Mg)O QWs do not mention the presence of such a field.

For type I QWs, where both electron and hole are confined in the same layer, the quantum-confined Stark effect (QCSE) red-shifts the fundamental optical transition. The internal electric field induces spatial separation of carriers having different charges. As a consequence, there is a decrease of the overlap between the electron and hole ground state wave functions that reduces the oscillator strength of the fundamental transition. It also reduces the exciton binding energy by loosening the Coulomb attraction that controls the extension of their in-plane relative motion. These effects have been observed in QWs [20,21] based on wurtzite group-III. Two regimes can be defined:

- For narrow QWs, the quantum confinement dominates; the emission energy is above the band gap and typical excitonic lifetimes of nanoseconds.

- For wide enough QWs, the QCSE dominates and the emission energy is below the band gap and decreases almost linearly with increasing Lw, up to a point, whereas the exciton lifetime increases exponentially.

In order to prevent these effects, it is possible to grow the quantum heterostructures along the so-called nonpolar directions, i.e. with the polar c-direction of ZnO lying in the growth plane. Wide ZnO/(Zn, Mg)O-based QWs without QCSE have been successfully grown on the a-plane (11-20) [13,22,23] or the m-plane (10-10) [24,25].

In this article, the experimental and theoretical work about the optical properties of excitons in ZnO/(Zn, Mg)O-based QWs grown by MBE are presented. We briefly introduce the various experimental techniques and samples used in Section 2. Section 3 is dedicated to optical properties of heterostructures grown according to the polar c-axis. The effects of the QCSE on the exciton recombination energy and lifetime as well as the radiative efficiency are discussed. The optical properties of homoepitaxial QW growth on m-plane ZnO are presented in Section 4. The last section is devoted to the conclusion.

2. Experimental detail

The samples are investigated by means of reflectance, continuous-wave photoluminescence (CW-PL), integrated time-resolved photoluminescence, and time-resolved photoluminescence (TRPL) experiments. The signal is collected and focused onto the entrance slit of the spectrometer. Two parabolic mirrors were used in order to suppress any achromatism. For reflectivity and CW-PL, the light sources are a Xenon lamp and a helium-cadmium laser at 325 nm, respectively. The photoluminescence and reflectivity signals are analyzed using a 550 mm monochromator equipped with a CCD-camera. For the TRPL experiments the excitation source is provided by the third harmonics of a Ti-sapphire laser, (λ = 266 nm), with pulse duration of 2 ps. A grating with 150 grooves/mm disperses the PL signal, which is then detected by a Hamamatsu synchroscan streak camera. The repetition rate of excitation pulses is adapted to the dynamics of each particular QW using an acousto-optic modulator, to prevent multiple excitations. Temperature dependence experiments are conducted using a helium flow cryostat. The temperature is controlled from 10 K to 325 K.

The QW samples are grown in a Riber Epineat MBE system equipped with effusion cells for Zn and

Mg elementals. The heteroepitaxial QW samples were grown on a 1-μm-thick ZnO template deposited on the c-plane of sapphire substrates. The samples contain 1 or 2 QWs separated by a very wide barrier of 200 nm. The homoepitaxial QW samples have identical designs. Their structure is made of the following layers: (Zn, Mg)O (200 nm) / ZnO (QW) / (Zn, Mg)O (50 nm) deposited on m-plane ZnO substrate. The Mg concentration is measured to be $\sim 20\%$ for all the samples.

3. Polar ZnO/(Zn, Mg)O-based quantum wells

Figure 1 shows the CW-PL spectra, recorded at 10 K, of the various investigated QWs with different width (Lw). The higher energy PL peak (3.8 eV) is consistent with the emission of $Zn_{1-x}Mg_xO$ barriers with x = 0.22 [5]. The direct evidence of the presence of a strong electric field is given by the PL lines of the 2 wider QWs, both of which lie below the ZnO excitonic gap. Moreover, it can be noted that the QW PL lines are accompanied by a series of longitudinal-optical phonon replicas, below the dominant peak. The intensity of the first phonon replica lines, relative to the zero-phonon line, increases when the width of the QW increases [8,26,27]. This is another effect of the electric field. For wide QWs the internal electric field separates the electron and hole wave functions along the c-axis. Consequently, a strong dipole is formed, which enhances the coupling with polar phonons.

The presence of large built-in electric fields in the QWs is evident also in the pump-power dependence of the emission energy as illustrated in Figure 2. This effect remains small in the narrower QWs, but it can be very large in the wider ones, as shown in Figure 2 for a QW with 7.1 nm width, where a blue-shift of ~ 80 meV is observed by increasing the pump power density over 6 orders of magnitude. The shift of the PL line results
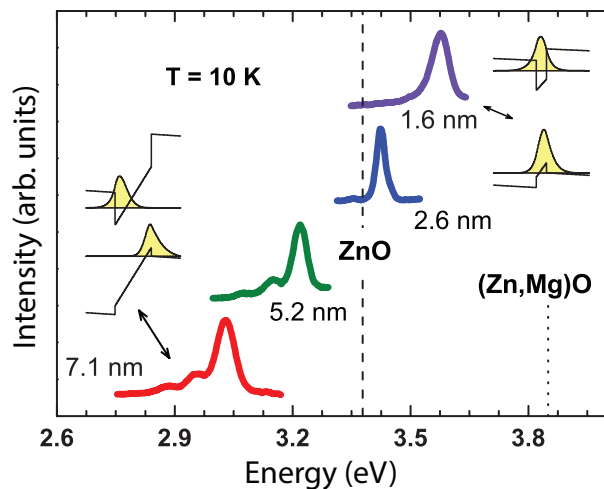
Figure 1. Time-integrated PL spectra of single ZnO/(Zn, Mg)O QWs of various widths taken at T = 10 K. Dashed lines show the energies of excitonic band gap of ZnO and (Zn, Mg)O. The inserts illustrate the effect of internal electric field on electron and hole wave function for a narrow and a wide QW.
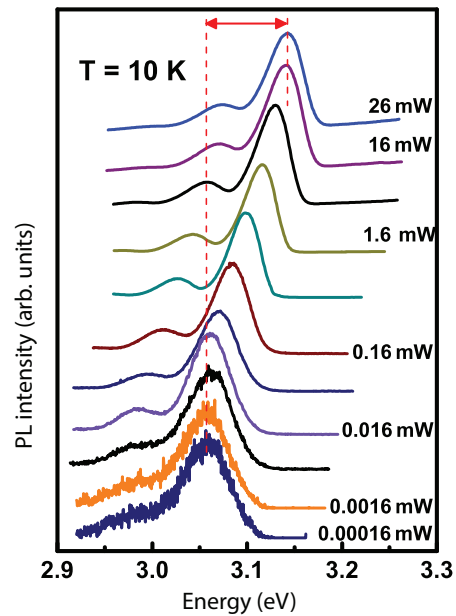
Figure 2. Continuous-wave PL spectra of the 7.1 nm QW recorded at low temperature, for various pump-power densities.

from the screening of the internal electric field by high densities of electron-hole dipoles. Such effects can also be produced for the wider QWs at moderate excitation densities because of the large recombination time as discussed below.

A prerequisite to determine the magnitude of the internal electric field is the knowledge of the minimum PL energy that the system can reach. In other words, we need to quantify as precisely as possible the values of PL energies that correspond to the case of unscreened internal electric fields. For this purpose, time-resolved PL measurements are very helpful. Figure 3 gives an example of the dynamics of the descreening of the internal electric field for a relatively wide QW. The most striking feature is the energy shift of the peak with time after the pulsed laser excitation. Initially, the spectrum peaks around 3.08 eV and, with time, a red shift is observed down to a value of 3.02 eV. This behavior is attributed to the screening and descreening of the internal electric field due to the electron-hole pairs concentration change along time [9,21,28,29]. Immediately after the pulse excitation, the density of electron-hole dipoles induces an effective electric field that opposes the internal one. The latter is thus partially screened and the PL line is blue-shifted in comparison to the very low excitation regime. The progressive loss of carriers after the excitation pulse due to recombination processes induces a descreening of the electric field and, hence, a red shift of the transition energies by restoration of the QCSE.

Indeed, the real value of the transition energy is obtained from time-integrated PL instead of CW-PL. The time-integration window is restricted to delays large enough to ensure the constancy of the emission energy. Moreover, the repetition rate is adapted to the slowness of the observed decay, in order to get a full deexcitation between 2 consecutive pulses. Using this careful procedure, the excitonic transition energy and exciton lifetime are measured. The results are presented in Figure 4. For narrow QWs, with width smaller than 3 nm, the exciton transition energies are higher than that of the ZnO bulk, and the lifetimes are in the order of nanoseconds. For these QWs, the quantum confinement effects dominate the exciton properties. For relatively wide QWs, with widths larger than 3 nm, the exciton transition energies are lower than those of the ZnO bulk and decrease linearly with the well width while at the same time the lifetime increases exponentially.
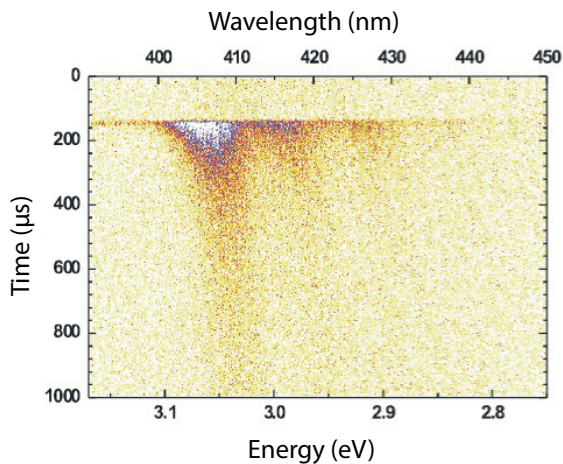
Figure 3. Image of the TRPL of the 7.1 nm thick ZnO/(Zn, Mg)O QW measured at T=10 K as measured by the streak camera apparatus.
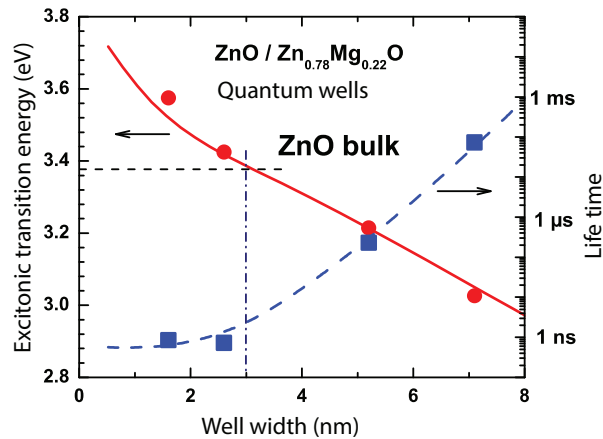
Figure 4. PL peak energies (circles) as a function of well width compared to the result of our variational calculation (solid curve). The dash-dotted lines show the excitonic gap of ZnO and the critical well width separating the 2 regimes of confinement (see text). The dashed curve shows the calculated exciton lifetime compared with the experimental PL decay times.

In order to determine the internal electric field from the experimental results, we have calculated the energy of the fundamental transition, the binding energy, and the oscillator strength of the ground-state exciton by a variational method [30,31] that includes the electric field. The numerical parameters used in the calculation are $m_e = 0.24$ and $m_h = 0.78$ for electron and hole on-axis effective masses and $\varepsilon_b = 6.4$ for the dielectric constant, in both well and barrier materials. These values are consistent with a ZnO exciton binding energy of 60 meV. The conduction-band offset ratio is taken at 0.8 [32].

In a QW without internal electric field, reducing the distance between the electron and the hole increases the interaction between the 2 particles. The binding energy is, in this case, higher than the bulk value. This is the typical effect of quantum confinement. Before going further, let us now examine the influence of the internal electric field on the exciton binding energy. For wider QWs the electric field pushes the electron and the hole towards either side of the QW, thus loosening their Coulombic binding. The exciton binding energy reduces when the width increases.

The dependence of the exciton radiative lifetime on well width is proportional, in this "one band" approximation, to the calculated quantity $f = |\varphi_\lambda(0)|^{-2} \left| \int_{-\infty}^{+\infty} dz\, f_e(z)\, f_h(z) \right|^{-2}$. To fit the measured PL decay times, f is simply multiplied by a unique coefficient. The calculation with an electric field of 0.9 MV/cm is in very good agreement with the experimental PL energies and lifetimes (Figure 4). It is important to note that the fitting electric field value really depends on the variation of the exciton binding energy.

The internal electric field in a ZnO/(Zn, Mg)O single QW [33] varies linearly with the magnesium concentration, x, with a coefficient of A = 3.95 (MV/cm). In the case of multiple QW systems, the distribution of the electric field among the well and barrier layers [34] should be taken into consideration. The resulting electric field in the QW is given by: $F_W = F_{\max} L_B/(L_B + L_W)$, where $F_{\max}$ is the maximum electric field. For samples having very thick barriers ($L_B \gg L_W$), it is obvious from this formula that the electric field in the well layer is close to $F_{\max}$. In contrast, relatively narrow barrier layers will significantly reduce the effective field in the QW.

The QCSE is harmful to optical properties of the QWs. The same also holds for the performance of optoelectronic devices based on these structures. A comparison between the radiative efficiency of 2 QWs separated by a barrier of 200 nm in width has been made by studying the variation of the PL integrated intensity as a function of temperature. Figure 5 shows that the nonradiative recombination channels dominate the excitonic recombination for the 2 QWs. For the QW with a width of 7.1 nm, the intensity of PL decreases by 2 orders of magnitude between 8 K and 50 K, while it is necessary to go to 300 K to observe the same variation of intensity for the QW with a 1.6 nm width. In a simple model the radiative efficiency (η), which is proportional to PL intensity (I_{PL}), is given by

$$I_{PL} \sim \eta = \frac{\tau_{nonrad}}{\tau_{nonrad} + \tau_{rad}},$$

where τ_{nonrad} and τ_{rad} are, respectively, the nonradiative and radiative decay times. The well-width dependence of the intensity as a function of temperature is due to the difference in radiative lifetime, which is 5 orders of magnitude higher for the wide QW than the thinner one.

4. Nonpolar ZnO/(Zn, Mg)O-based quantum wells

The growth of QWs on nonpolar planes, such as the m-plane (10-10) or a-plane (11-20), has been proposed in order to avoid the QCSE. Here, there is no component for spontaneous fields of polarization in these orientations

because the polar c-axis lies on the growth plane. In this paper, we focus only on the optical properties of several homoepitaxial ZnO/(Zn, Mg)O single QWs grown on m-plane ZnO substrate.

The reflectance and CW-PL spectra [24,35] reveal strong in-plane optical anisotropies, as predicted by group theory. In reflectance, the spectral signature of confined excitons built from spin-orbit split-off band in the valence band, analogous to the C-exciton in bulk ZnO, is detected using light polarized along the c-axis. Confined states analogous to A and B bulk excitons are detected in experiments performed in orthogonal polarization.

Figure 6 summarizes the low temperature (10 K) reflectance (open symbols) and CW-PL (closed symbols) study of a series of single QWs with widths ranging from 1.3 to 6.2 nm. The most important feature here is that the exciton transition energy is above the value of that of the bulk material, independent of the well width, indicating that there is no internal electric field in these structures. The weak Stokes shift between PL and reflectivity is a measure of reasonable smoothness of heterointerfaces with terraces of the size of the exciton Bohr radius or larger [25]. The envelope function calculations, which include excitonic interaction (solid line), nicely match the experimental results.
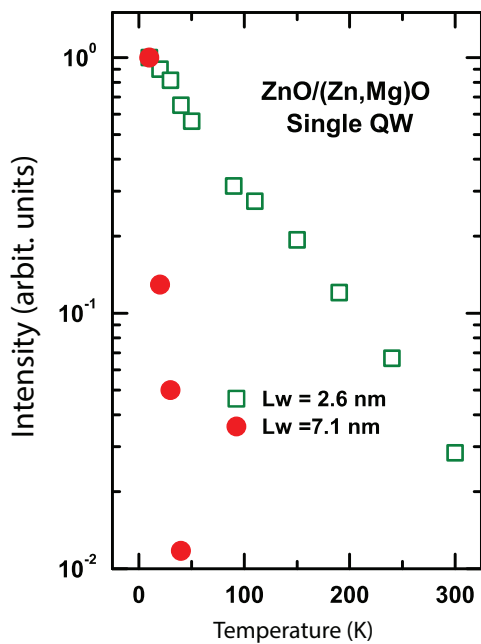

Figure 5. Evolution of the intensities of CW-PL normalized for 2 QWs having respective widths of 2.6 nm (open squares) and 7.1 nm (full circles) as function of temperature.
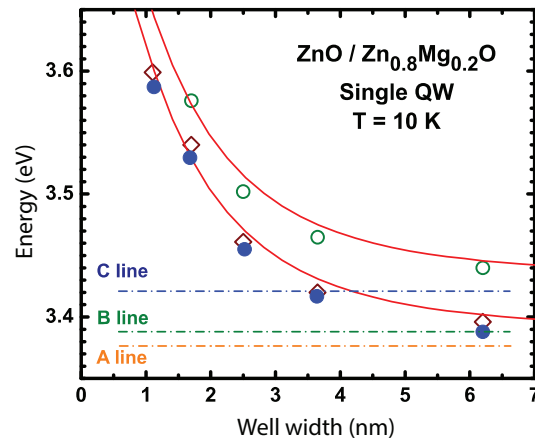

Figure 6. Transition energies are plotted versus well width for a series of M-plane oriented ZnO/(Zn, Mg)O single QWs. In reflectance spectra signatures of excitons (open circles), analogous to C-exciton in bulk ZnO, are detected using a light polarized along the c-axis. The energies of states analogous to A and B bulk excitons are extracted respectively from PL (full circles) and reflectance (open squares) experiments performed in orthogonal polarization. Dashed lines indicated the energies of the excitons in the bulk ZnO. Solid lines represent the result of the effective mass envelope function calculation, including hole-electron interactions.

Figure 7a shows a series of CW-PL spectra measured at different temperatures ranging from 10 K to 300 K. It is interesting to note the reversal of intensities between the 2 peaks associated with free and localized excitons, which indicates an efficient detrapping of the bound exciton. A clear splitting between the 2 lines is observed up to 250 K, and then they merge to form a broad luminescence band. A deconvolution procedure of the photoluminescence band is performed in order to extract the intensity of the 2 peaks. It is worth noting that the total photoluminescence intensity (Figure 7b) does not collapse with increasing temperature. This is a clear indication that nonradiative processes in this sample are not efficient even beyond room temperature, which is extremely promising for optoelectronic devices. This remarkable property is confirmed by measurement of the lifetime of free and localized excitons by TRPL. Both decay times show identical behavior with temperature (Figure 8). They increase linearly from $\sim$750 ps to $\sim$2.4 ns when the temperature increases from 100 K to room temperature. This linear increase of the decay time is typical of free excitons in QWs. The slope of about 7 ± 1 ps/K is elaborated on in detail in a previous study [25].
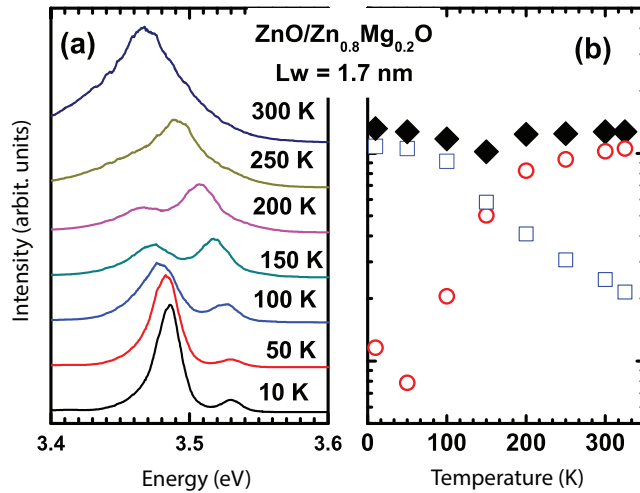
Figure 7. **(a)** Evolution of the PL spectra of a 1.7-nm-thin ZnO/(Zn, Mg)O single quantum well grown on an M-plane oriented ZnO substrate as a function of temperature. The 2 lines correspond to confined free excitons (3.53 eV at 10 K) and localized excitons (3.48 eV at 10 K). Note the population exchange between the 2 lines. **(b)** Intensity of free (open square) and localized (open circle) exciton PL lines for different temperatures. Note that the total intensity (close symbol) does not change when temperature increases.
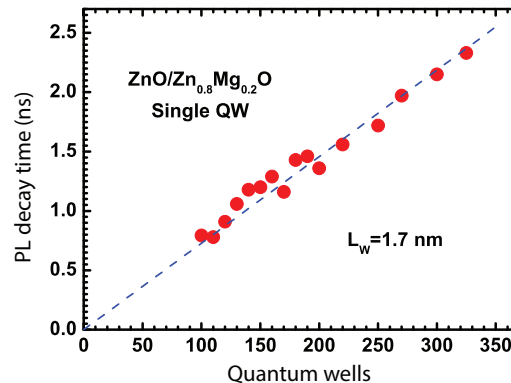
Figure 8. PL decay times of the localized and free excitons versus temperature. The slope of the straight line is about 7 ± 1 ps/K.

5. Conclusions

The optical properties of ZnO-based QWs are presented. For single QWs grown along the (0001) axis, the fundamental importance of the QCSE on the exciton's recombination energy and oscillator strength as well as radiative efficiency has been treated through the discussion of CW-PL and TRPL experimental results. Most of the detrimental effects of the QCSE can be avoided by using QWs grown on nonpolar planes. In the latter case, reflectance, CW-PL, and TRPL properties of single QWs grown on m-plane oriented ZnO substrates have revealed both free excitons (with a weak Stokes shift between the reflectance and photoluminescence spectra) and localized excitons. The temperature dependence of the intensity of the photoluminescence indicates a very moderate contribution from nonradiative recombination channels in these samples. The radiative decay times of the free excitons and of the localized excitons have been monitored as a function of temperature. Above 100 K the decay times of both free and localized excitons have identical values and similar rates of change dependence on T. Such high-quality QWs open up possibilities for UV optoelectric devices. However, an important obstacle still remains in effect, which must be overcome so that the ZnO can make a breakthrough in the world of devices: the attainment of p-type conductivity in ZnO.

References

[1] Morkoç, H.; Özgür, U. *Zinc Oxide: Fundamentals, Materials and Device Technology*; Weinheim: Wiley-VCH, 2009.

[2] Özgür, U.; Alivov, Y. I.; Liu, C.; Teke, A.; Reshchikov, M. A.; Doğan, S.; Avrutin, V.; Cho, S. J.; Morkoç, H. *J. Appl. Phys.* **2005**, *98*, 041301.

[3] Ohtomo, A.; Kawasaki, M.; Sakurai, Y.; Ohkubo, I.; Shiroki, R.; Yoshida, Y.; Yasuda, T.; Segawa, Y.; Koinuma, H. *Mater. Sci. Eng. B* **1998**, *56*, 263–266.

[4] Makino, T.; Chia, C. H.; Tuan, N. T.; Sun, H. D.; Segawa, Y.; Kawasaki, M.; Ohtomo, A.; Tamura, K.; Koinuma, H. *Appl. Phys. Lett.* **2000**, *77*, 975–977.

[5] Makino, T.; Segawa, Y.; Kawasaki, M.; Ohtomo, A.; Shiroki, R.; Tamura, K.; Yasuda, T.; Koinuma, H. *Appl. Phys. Lett.* **2001**, *78*, 1237–1239.

[6] Makino, T.; Isoya, G.; Segawa, Y.; Chia, C. H.; Yasuda, T.; Kawasaki, M.; Ohtomo, A.; Tamura, K.; Koinuma, H. *J. Cryst. Growth* **2000**, *214*, 289–293.

[7] Sun, H. D.; Makino, T.; Segawa, Y.; Kawasaki, M.; Ohtomo, A.; Tamura, K.; Koinuma, H. *Appl. Phys. Lett.* **2001**, *78*, 3385–3387.

[8] Makino, T.; Tamura, K.; Chia, C.; Segawa, Y.; Kawasaki, M.; Ohtomo, A.; Koinuma, H. *Phys. Rev. B,* **2002** *66*, 233305.

[9] Makino, T.; Segawa, Y.; Tsukazaki, A.; Ohtomo, A.; Kawasaki, M. *Appl. Phys. Lett.* **2008**, *93*, 121907.

[10] Makino, T.; Segawa, Y.; Tsukazaki, A.; Saito, H.; Takeyama, S.; Akasaka, S.; Nakahara, K.; Kawasaki, M. *Phys. Rev. B* **2013**, *87*, 085312.

[11] Zhang, B. P.; Binh, N. T.; Wakatsuki, K.; Liu, C. Y.; Segawa, Y.; Usami, N. *Appl. Phys. Lett.* **2005**, *86*, 032105.

[12] Gruber, T.; Kirchner, C.; Kling, R.; Reuss, F.; Waag, A. *Appl. Phys. Lett.* **2004**, *84*, 5359–5361.

[13] Chauveau, J. M.; Laügt, M.; Vennegués, P.; Teisseire, M.; Lo, B.; Deparis, C.; Morhain, C.; Vinter, B. *Semicond. Sci. Technol.* **2008**, *23*, 035005.

[14] Chauveau, J. M.; Morhain, C.; Teisseire, M.; Laügt, M.; Deparis, C.; Zuniga-Perez, J.; Vinter, B. *Microelectron. J.* **2009**, *40*, 512–516.

[15] Sadofev, S.; Blumstengel, S.; Cui, J.; Puls, J.; Rogaschewski, S.; Schäfer, P.; Sadofyev, Y. G.; Henneberger, F. *Appl. Phys. Lett.* **2005**, *87*, 091903.

[16] Chauveau, J. M.; Teisseire, M.; Kim-Chauveau, H.; Deparis, C.; Morhain, C.; Vinter, B. *Appl. Phys. Lett.* **2010**, *97*, 081903.

[17] Gopal, P.; Spaldin, N. A. *J. Electron. Mater.* **2006**, *35*, 538–542.

[18] Malashevich, A.; Vanderbilt, D. *Phys. Rev. B* **2007**, *75*, 045106.

[19] Park, S. H.; Ahn, D. *Appl. Phys. Lett.* **2005**, *87*, 253509.

[20] Bretagnon, T.; Lefebvre, P.; Valvin, P.; Bardoux, R.; Guillet, T.; Taliercio, T.; Gil, B.; Grandjean, N.; Semond, F.; Damilano, B. et al. *Phys. Rev. B* **2006**, *73*, 113304.

[21] Lefebvre, P.; Kalliakos, S.; Bretagnon, T.; Valvin, P.; Taliercio, T.; Gil, B.; Grandjean, N.; Massies, J. *Phys. Rev. B* **2004**, *69*, 035307.

[22] Chauveau, J. M.; Morhain, C.; Lo, B.; Vinter, B.; Vennéguès, P.; Laügt, M.; Buell, D.; Tesseire-Doninelli, M.; Neu, G. *Appl. Phys. A* **2007**, *88*, 65–69.

[23] Lautenschlaeger, S.; Eisermann, S.; Hofmann, M. N.; Roemer, U.; Pinnisch, M.; Laufer, A.; Meyer, B. K.; von Wenckstern, H.; Lajn, A.; Schmidt, F. et al. *J. Cryst. Growth* **2010**, *312*, 2078–2082.

[24] Béaur, L.; Bretagnon, T.; Gil, B.; Guillet, T.; Brimont, C.; Tainoff, D.; Teisseire, M.; Chauveau, J. M. *Phys. Status Solidi C* **2012**, *9*, 1320–1324.

[25] Béaur, L.; Bretagnon, T.; Gil, B.; Kavokin, A.; Guillet, T.; Brimont, C.; Tainoff, D.; Teisseire, M.; Chauveau, J. M. *Phys. Rev. B* **2011**, *84*, 165312.

[26] Béaur, L.; Bretagnon, T.; Guillet, T.; Brimont, C.; Gallart, M.; Gil, B.; Gilliot, P.; Morhain, C. *J. Lumin.* **2013**, *136*, 355–357.

[27] Sun, H. D.; Segawa, Y.; Kawasaki, M.; Ohtomo, A.; Tamura, K.; Koinuma, H. *J. Appl. Phys.* **2002**, *91*, 6457–6460.

[28] Chernikov, A.; Schäfer, S.; Koch, M.; Chatterjee, S.; Laumer, B.; Eickhoff, M. *Phys. Rev. B* **2013**, *87*, 035309.

[29] Stölzel, M.; Müller, A.; Benndorf, G.; Brandt, M.; Lorenz, M.; Grundmann, M. *Phys. Rev. B* **2013**, *88*, 045315.

[30] Morhain, C.; Bretagnon, T.; Lefebvre, P.; Tang, X.; Valvin, P.; Guillet, T.; Gil, B.; Taliercio, T.; Teisseire-Doninelli, M.; Vinter, B. et al. *Phys. Rev. B* **2005**, *72*, 241305(R).

[31] Gil, B.; Lefebvre, P.; Bretagnon, T.; Guillet, T.; Sans, J.; Taliercio, T.; Morhain, C. *Phys. Rev. B* **2006**, *74*, 153302.

[32] Senger, R.; Bajaj, K. *Phys. Rev. B* **2003**, *68*, 205314.

[33] Bretagnon, T.; Lefebvre, P.; Guillet, T.; Taliercio, T.; Gil, B.; Morhain, C. *Appl. Phys. Lett.* **2007**, *90*, 201912.

[34] Leroux, M.; Grandjean, N.; Massies, J.; Gil, B.; Lefebvre, P.; Bigenwald, P. *Phys. Rev. B* **1999**, *60*, 1496–1499.

[35] Béaur, L.; Bretagnon, T.; Brimont, C.; Guillet, T.; Gil, B.; Tainoff, D.; Teisseire, M.; Chauveau, J. M. *Appl. Phys. Lett.* **2011**, *98*, 101913.